International Journal of Microwave and Wireless Technologies

cambridge.org/mrf

An efficient method for three-dimensional through-the-wall radar imaging

Akhilendra Pratap Singh[1] and Vineet Singh[2]

[1]Department of Electronics and Communication Engineering, Indian Institute of Information Technology, Bhopal, India and [2]Department of Electronics and Communication Engineering, National Institute of Technology Patna, Patna, India

Research Paper

Cite this article: Singh AP, Singh V (2026) An efficient method for three-dimensional through-the-wall radar imaging. *International Journal of Microwave and Wireless Technologies* **18**(2), 199–211. https://doi.org/10.1017/S1759078726103006

Received: 26 August 2025
Revised: 10 February 2026
Accepted: 11 February 2026

Keywords:
3D through-the-wall radar imaging; autofocusing technique; real-time radar imaging

Corresponding author:
Akhilendra Pratap Singh;
Email: asingh@iiitbhopal.ac.in

Abstract

In three-dimensional (3D) through-the-wall radar imaging, unknown wall parameters such as thickness and relative permittivity distort electromagnetic wave propagation, causing image defocusing and target displacement. Autofocusing is therefore essential, but conventional methods are computationally demanding due to two-dimensional (2D) searches over wall parameters and repeated reconstruction of full 3D images. To address this challenge efficiently, a slice-based 3D imaging strategy is adopted. Radar data are acquired along a linear aperture parallel to the wall at multiple heights. For each height, the collected measurements form a B-scan dataset, which is processed independently to reconstruct a 2D image slice. A computationally efficient two-step framework is proposed. First, the wall's relative permittivity is estimated from the time-domain response of the B-scan at a selected height, and autofocusing is performed by varying only the wall thickness, reducing the conventional 2D search to a one-dimensional problem. Second, focused 2D image slices are reconstructed at all heights. The final 3D image of the concealed targets is obtained by superimposing these slices into a volumetric representation. The experimental results demonstrate that the proposed technique yields well-focused images while significantly reducing the computational cost.

Introduction

Through-the-wall radar imaging (TWRI) is a system that uses electromagnetic waves to detect and locate objects behind walls [1]. In recent years, TWRI has gained increasing popularity in both military, search and rescue, and security applications [1]. One of the several challenges that exist in TWRI is the development of through-the-wall imaging algorithm with unknown wall parameters for synthetic aperture radar (SAR) to generate three-dimensional (3D) images of the scene behind the wall [1]. In practice, wall parameters are unknown or known with some degree of uncertainty. Using incorrect wall parameters during imaging can defocus the reconstructed image, leading to blurred or displaced target representations [2].

Many autofocusing methods have been proposed for SAR to generate focused images when wall parameters are unknown. These methods can generally be grouped into three categories. The first category comprises trajectory-based approaches, which require two or more distinct array structures and are therefore time-consuming [3–7]. The second category involves estimating wall parameters prior to imaging [8–16]. In this case, unknown parameters can be retrieved through optimization techniques that minimize the mismatch between measured and predicted values, such as the reflection coefficient [9]. However, this process is often more complex than imaging itself and heavily depends on the accuracy of the modeling [3]. A simpler method for estimating the wall transmission coefficient has been introduced in Ref. [10], which avoids optimization but requires a multistatic configuration. In addition, direct estimation approaches that infer wall parameters directly from the reflected fields without optimization have also been reported [11–16]. The third category focuses on image quality optimization, which generally provides superior performance and has been widely adopted [8]. It is an iterative method that adjusts parameters based on a focus evaluation function until the image with the optimal focus is achieved [17–22]. Traditional imaging processing of the third kind of methods involves discretizing the defined search range for wall thickness and relative permittivity into equal intervals to generate all possible wall thickness and relative permittivity parameter pairs. For each pair, a radar image is formed and evaluated using a focusing metric. This process of image reconstruction and evaluation is performed for all parameter pairs. Then, the image corresponding to the pair with the best focusing metric is selected as the final focused image. Owing to this exhaustive image formation and evaluation process for all possible pairs, the imaging process described in Refs [17–20] poses a significant computational burden. To reduce the computational burden, some methods based on image domain filter and parametric sparse representation have

© The Author(s), 2026. Published by Cambridge University Press in association with The European Microwave Association.

been proposed [3, 21, 22]. However, they still required a two-dimensional (2D) search over wall parameters, typically wall thickness and relative permittivity, which represents a large computational burden. Therefore, a more computationally efficient method is desirable.

This paper presents an efficient autofocusing method for the SAR-based 3D through-the-wall image formation, which will transform a 2D searching procedure into a one-dimensional (1D). Instead of adjusting both parameters, our method first estimates the wall's relative permittivity using time-domain signals reflected from the front side of the wall. Then, it focuses on fine-tuning just one parameter, wall thickness, to create an optimal radar image. Thus, the proposed autofocusing method will transform a 2D searching procedure into a 1D problem. By reducing the process to a single adjustable parameter, our method is faster and uses fewer computational resources compared to traditional methods. This new approach is a major improvement because it simplifies the process while maintaining high image quality. It is especially useful for real-time radar systems, where quick and efficient imaging is essential. By narrowing the focus to one parameter and accurately estimating permittivity, our method is a practical and effective solution to the challenges of traditional autofocusing techniques. However, the effectiveness of the proposed method depends on an accurate initial estimate of ε_r and relies on modeling the wall as a single homogeneous layer, thereby limiting its applicability to thin or multilayered wall scenarios. The structure of the article is as follows: The "Proposed method" section describes the proposed novel real-time autofocusing algorithm, the "Experimental results" section presents simulation and experimental results to validate the method, while the "Conclusion" section presents the conclusion.

Proposed method

To efficiently address the 3D TWRI problem, a 2D slice-based imaging strategy is employed [9]. In this approach, data are acquired along a linear aperture parallel to the wall at multiple heights. For a given height, the measurements recorded as a function of antenna position and frequency form a B-scan dataset. Each B-scan is processed independently to reconstruct a 2D image slice corresponding to that height. A two-step imaging framework is proposed for through-the-wall scene reconstruction. In the first step, the wall thickness and dielectric permittivity are estimated from the B-scan data at a selected height using a simple and computationally efficient method. In the second step, 2D image slices are reconstructed at all heights. Finally, the 3D representation of the concealed scatterers is obtained by superimposing the individual 2D slices, resulting in a volumetric image of the scene.

In this section, we present the proposed two-stage autofocusing approach for 2D radar image formation from B-scan data. The main steps of the proposed method are shown in Fig. 1. The proposed method involves estimating the wall's relative permittivity, followed by optimizing the 2D radar image by adjusting the wall thickness. The primary goal is to enhance image quality by iteratively refining the wall thickness based on estimated parameters. First, the value of the first peak P_{t1} coming from the first interface from the others will be separated to estimate the relative permittivity. In order to obtain a good estimation of relative permittivity, the signal should not take into account all the wall reflections but only the one coming from the first interface; otherwise, the relationship between relative permittivity and the reflection coefficient is more complicated and depends on the wall thickness. Next, an autofocusing method is used to obtain optimal 2D radar image by adjusting only the wall thickness parameter in each iteration, only the wall thickness is adjusted, and 2D radar images are generated using the updated wall thickness and estimated relative permittivity values. The image corresponding to this optimal thickness, achieved when the image quality parameter is maximized, is retained as the final output of the through-the-wall imaging result. Although there are several approaches for image formation, we employed delay and sum beamforming due to low computational load. This section first outlines the method for estimating the wall's relative permittivity, followed by the autofocusing approach for image formation.

Stage 1: estimating the wall's relative permittivity

Consider a stepped frequency continuous wave radar positioned at a standoff distance d from a wall, illuminating an infinitely long, homogeneous, smooth wall from a sufficient distance, as shown in Fig. 2. The radar transmits and receives the magnitude and phase of reflected signals over a frequency range from $f_{\min}$ to $f_{\max}$ across N frequency points at mth scan position. The received frequency domain data is then converted into the equivalent time domain using the standard inverse fast Fourier transform.

The antenna is placed in the far-field relative to the wall, ensuring that a transverse electromagnetic (TEM) wave is normally incident on the wall. When the wave impinges on the front surface, as shown in Fig. 2, a portion of the wave is reflected due to the permittivity discontinuity at the interface, while the remaining portion propagates into the wall. The backscattered signal from a single-layer homogeneous wall primarily consists of time-shifted and attenuated replicas of the transmitted pulse, with the first two dominant echoes arising from the front and rear wall interfaces. While real building materials are indeed inhomogeneous, prior studies have shown that when the characteristic size of inhomogeneities is smaller than the system's pulse resolution, the wall can be accurately modeled as a homogeneous medium with an effective permittivity [23]. Under these conditions, the backscattered signal closely resembles that of an ideal homogeneous wall, and the dominant reflections still originate from the two interfaces, validating the underlying assumption used in our method. We also assume negligible material dispersion over the operating bandwidth, allowing the effective permittivity to be treated as frequency-independent. The first peak at time t_1 represents the received power P_{t1} of the wave reflected from the front surface of the wall. This formulation utilizes only the power quantity to determine the wall's relative permittivity. The received power P_{t1} is a function of the reflection coefficient Γ and the reference incident power P_{i}, as described by the following equations [22]:

$$P_{t1} \cong |\Gamma|^2 P_{\mathrm{i}} \tag{1}$$

The magnitude of the reflection coefficient can be calculated using the following equation [22]:

$$|\Gamma| \cong \sqrt{\frac{P_{t1}}{P_{\mathrm{i}}}} \tag{2}$$

Once the magnitude of the local reflection coefficient is obtained, the relative permittivity of the wall ε_r can be calculated using the following expression [22]:

$$\varepsilon_r = \left(\frac{1+|\Gamma|}{1-|\Gamma|}\right)^2 \tag{3}$$

In general, the reflection coefficient at a dielectric interface depends on both the relative permittivity ε_r and the loss tangent

https://doi.org/10.1017/S1759078726103006 Published online by Cambridge University Press

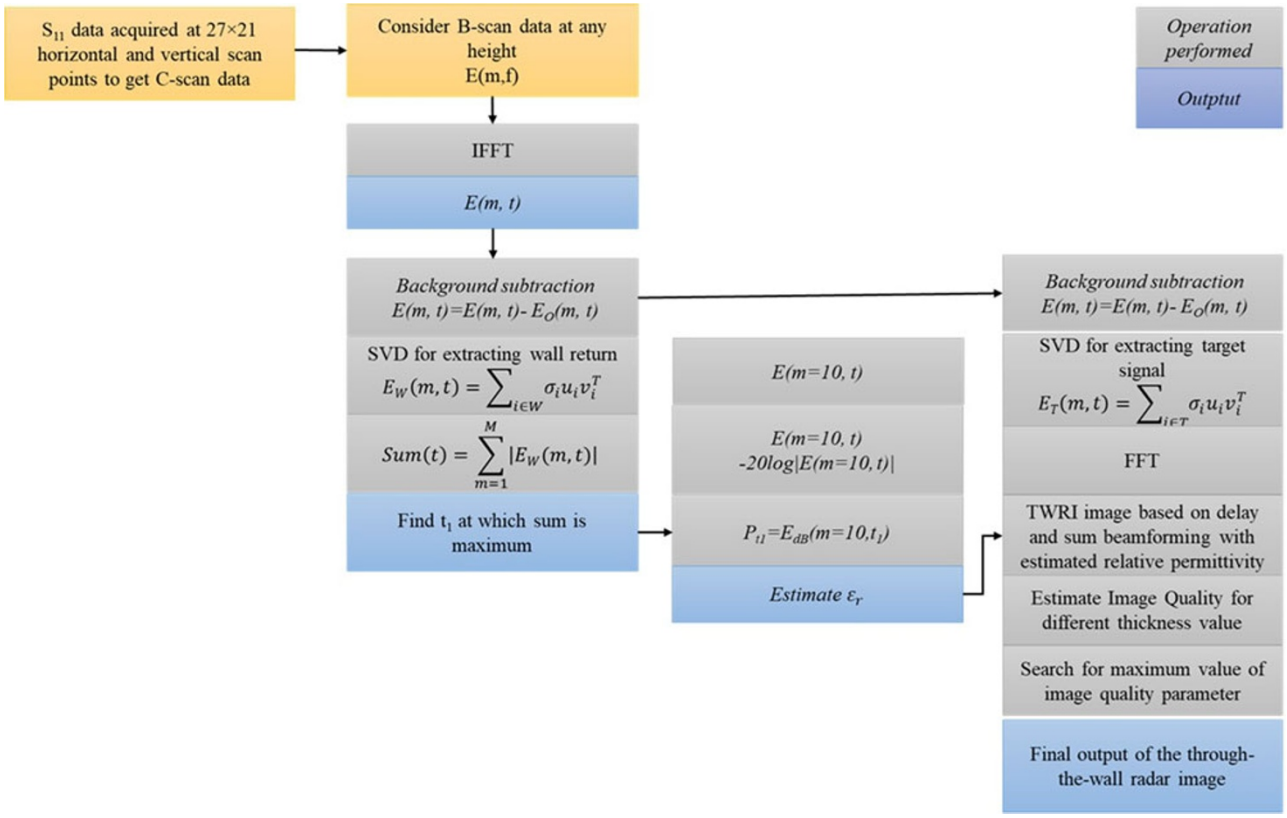


Figure 1. Flowchart of the proposed method.

tan δ. However, in this work, we adopt the standard assumption commonly used in TWRI studies that typical building materials are either lossless or only weakly lossy within the operating frequency band. As noted in Ref. [23], when the loss tangent is small, the propagation velocity is mainly governed by the real part of the permittivity, and the influence of the loss tangent becomes negligible. Consequently, under weak-loss conditions, the effect of tan δ on both the phase and magnitude of the reflection coefficient is minor compared to the dominant contribution of ε_r. Therefore, within the low-loss approximation, the reflection coefficient can be treated primarily as a function of the permittivity.

The wall's relative permittivity can be determined by exploiting P_{t1} at time point t_1 from the time-domain plot. The separation of the first echo from the reflections arising at subsequent interfaces is a critical step for accurately estimating the relative permittivity using Equation (3). **Step 1 – Frequency to time domain conversion**: The frequency domain data $E(m, f)$ is converted into time-domain data E (m, t) by applying the inverse fourier transform. This gives the time-domain response at each scan point for all time values. **Step 2 – Background subtraction**: Background subtraction is applied to remove the antenna mismatch reflection from measured TWRI data.

$$E(m,t) = E(m,t) - E_O(m,t)\,, \tag{4}$$

where $E(m, t)$ represents the measured time-domain data at the mth scan point and tth time instance, $E_O(m, t)$ represents the reference measurement performed in an anechoic chamber to account for antenna mismatch. This step ensures that the signal contains only the reflections due to the wall and targets. **Step 3 – Singular value decomposition (SVD)**: SVD is performed to isolates the dominant wall reflection from other background components. Experimental findings in Ref. [24] demonstrate that SVD decomposes the time-domain data matrix into orthogonal singular vectors, where the dominant singular values correspond to the strongest reflections, typically from the wall, while the weaker singular values capture reflections from the target. When the wall and target echoes exhibit distinct temporal and spatial characteristics, they are mapped onto separate singular vectors, effectively ensuring their orthogonality. Wall reflections tend to be significantly stronger than target reflections due to the wall's high reflectivity and larger surface area. This disparity in signal strength causes the wall subspace to dominate the leading singular values, whereas target echoes are represented in lower-energy singular components. A threshold can be set on the singular value spectrum to distinguish dominant components (associated with the wall) from non-dominant ones (representing the target and noise). Otsu's method is commonly employed to identify the optimal threshold by maximizing the variance between these classes. For this, the time-domain data $E(m, t)$ is decomposed using SVD into the wall subspace $E_W(m,t)$ and target subspace $E_T(m,t)$. The wall subspace component is selected based on Otsu's method, which contains most of the wall reflection such that [24]

$$E_W(m,t) = \sum_{i\in W}\sigma_i u_i v_i^T\,, \tag{5}$$

where σ_i represent singular values arranged in decreasing order, i.e. $\sigma_1 > \sigma_2 > \ldots > \sigma_N > 0$, u_i and v_i represent left and right singular vectors. **Step 4 – Finding P_{t1} and relative permittivity**:

https://doi.org/10.1017/S1759078726103006 Published online by Cambridge University Press

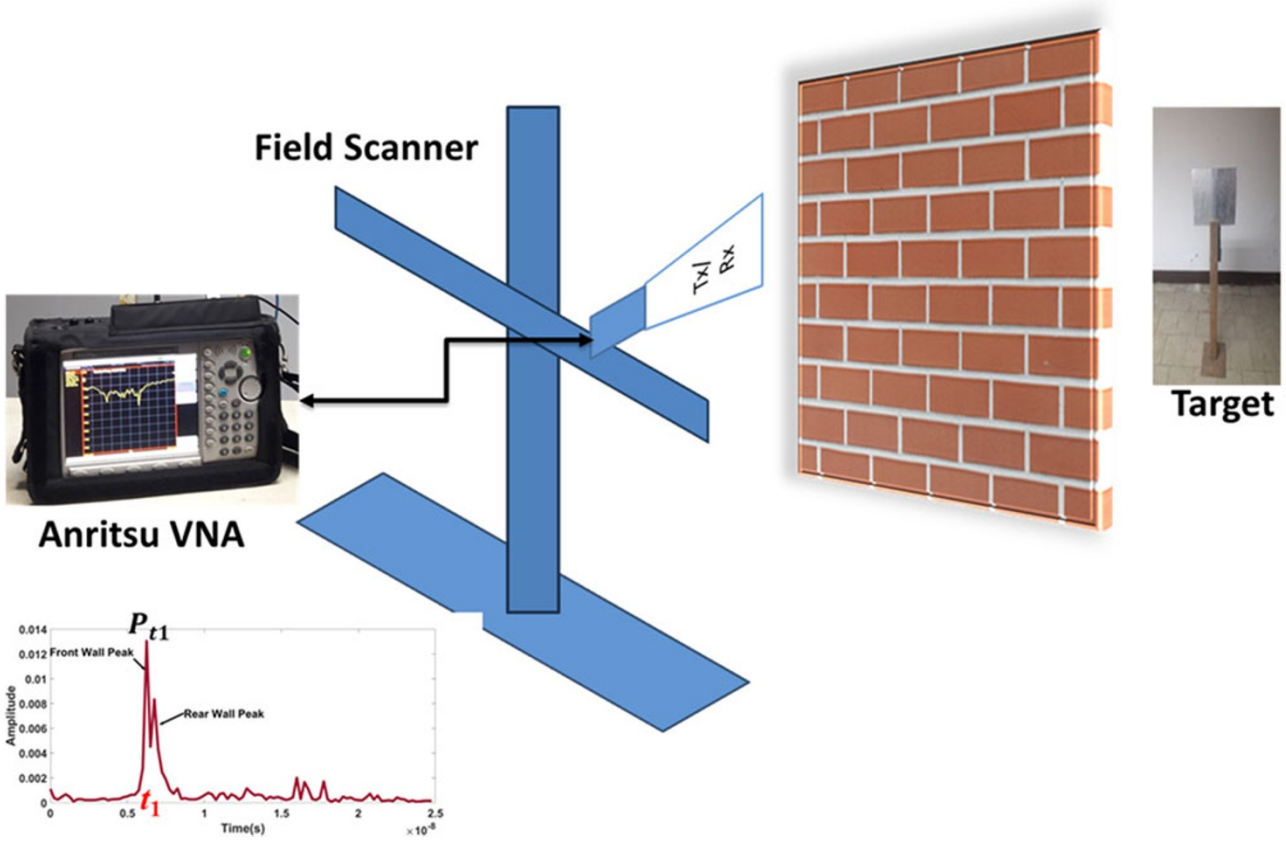


Figure 2. Through-the-wall image scene.

First, $S_W(m,t)$ are added up in the time domain given as

$$\sum(t) = \sum_{m=1}^{M} |E_W(m,t)| \tag{6}$$

Next, find the index value t_1 at which the sum is maximum, which corresponds to the time when the first echo is most pronounced in time domain profile. Then, find P_{t1} at time points t_1 from time-domain profile of any one scan point, say $m = 10$.

$$P_{t1} = E(m = 10, t_1) \tag{7}$$

Stage 2: autofocusing method is employed to generate a focused image

Once the relative permittivity is estimated, time-domain data $E_T(m,t) = \sum_{i \in T} \sigma_i u_i v_i^T$ representing the target subspace converted can be converted to the frequency domain. The delay and sum beamforming algorithm can be applied to frequency domain data. Using the estimated relative permittivity, an image quality optimization scheme can be applied to recursively autofocus the images. In each iteration, the assumed wall thickness value is modified, and a new beamformed image is generated based on the updated wall thickness. According to the delay and sum beamforming imaging algorithm, the value for the (x, y) pixel ($x = 1, 2, \ldots, Nx$; $y = 1, 2, \ldots, Ny$) is determined by [24]

$$I(x,y) = \frac{1}{MN} \sum_{m=1}^{M} \sum_{n=1}^{N} k_{m,n} \exp(j2\pi f_n \tau_m(x,y)) \tag{8}$$

Here, $\tau_m(x,y)$ represents the focusing delay between the mth scan point and the target situated at the pixel position (x, y). This focusing delay can be calculated using Snell's law, along with the distance from the transceiver to the front wall and the distance from the target to the back wall (see Ref. [22]). The signal received at the mth antenna location and the nth frequency, denoted as $z_{m,n}$, is given by [24]

$$k_{m,n} = \sum_{r=1}^{R} \sigma_r(f_n) \exp(-j2\pi f_n \tau_{m,r}) \tag{9}$$

$\sigma_r(f_n)$ represents the reflection coefficient of the rth target at the nth frequency, while $\tau_{m,r}$ denotes the round-trip travel time of the signal from the mth antenna location to the rth target location. It is well established that using an incorrect wall thickness value for imaging leads to decreased image resolution and causes the target to shift from its true position [2], resulting in reduced contrast in the resulting image. To obtain the optimal thickness value and the corresponding image, we use a well-known metric to measure the quality of a focused image, which is the higher-order moment of the image and is given by

$$M = \frac{1}{n} \sum_{i=1}^{n} (x_i - \bar{x})^5 \tag{10}$$

where n represents the no. of pixels, m is the order of the moment, x_i is the ith data value, and $\bar{x}$ is the mean of the data values. The optimal thickness can then be determined by identifying the maximum value of the moment. The image corresponding to this optimal

https://doi.org/10.1017/S1759078726103006 Published online by Cambridge University Press

thickness value, where the moment in Eq. (10) is maximized, is saved as the output of the 2D radar image results.

Experimental results

In this section, the proposed method for 2D image formation is first validated using synthetic data. The B-scan dataset was generated for a monostatic SAR system positioned at a standoff distance of 1 m from the wall and operating at a center frequency of 4.5 GHz with a bandwidth of 2 GHz and a frequency step of 10 MHz. Electromagnetic simulations were carried out using CST Microwave Studio. The antenna was scanned horizontally from −0.65 m to 0.65 m with a step size of 0.05 m. Two different TWRI scenarios were considered.

In Scene 1, the wall had a relative permittivity of $\varepsilon_r = 2.5$ and a thickness of 0.10 m, whereas in Scene 2, the wall permittivity was relative permittivity $\varepsilon_r = 6.5$ and a thickness of 0.30 m. In both cases, two targets were located behind the wall at positions (0.25, 1.42 m) and (−0.25, 2.17 m). The reconstruction process began with the estimation of the wall's relative permittivity, followed by an iterative autofocusing procedure in which the wall thickness was treated as the optimization parameter.

Using Steps 1–4, the first reflected wall peak P_{t1} for both scenes was identified at the time instant t_1. B-scan data were transformed to the time domain, and background subtraction was performed using Steps 1 and 2. In Step 3, the time-domain data were decomposed into wall and target subspace components. Step 4 was then applied to compute Sum(t) from the wall subspace and determine t_1 by locating the time at which Sum(t) reached its maximum. In Step 5, P_{t1} was obtained as $P_{t1} = S(m, t_1)$, and the wall's relative permittivity was subsequently estimated.

With the estimated permittivity, image reconstructions were carried out using 14 scan positions and 101 frequency bins while varying the wall thickness from 0.05 to 0.35 m in steps of 0.01 m. For each assumed thickness, the moment value was computed, and the image corresponding to the maximum moment value was selected as the optimally focused result. The reconstructed images for different wall thicknesses in Scenes 1 and 2 are shown in Figs 3(a) and 4(a), respectively. For Scene 1, the maximum moment occurred at the true wall thickness of 0.10 m, while for Scene 2 it was observed at 0.30 m. Reconstructions obtained using incorrect thickness values, shown in Figs 3(b–c) and 4(b–c), exhibit noticeable defocusing and smearing compared to the sharply focused images obtained at the correct wall thickness.

The results presented in Figs 4(a) and 5(a) were generated using noise-free data. To assess the robustness of the proposed approach, 20% additive random noise was introduced into the simulated dataset. The corresponding reconstructions, shown in Figs. 5(a) and 5(b), remain comparable to the noise-free case. Moreover, the moment curves plotted over different wall thickness values in Figs. 5(c) and 5(d) display similar trends under varying noise conditions, with the maximum moment consistently occurring at the true wall thickness for both scenes, thereby demonstrating the strong noise robustness of the proposed algorithm.

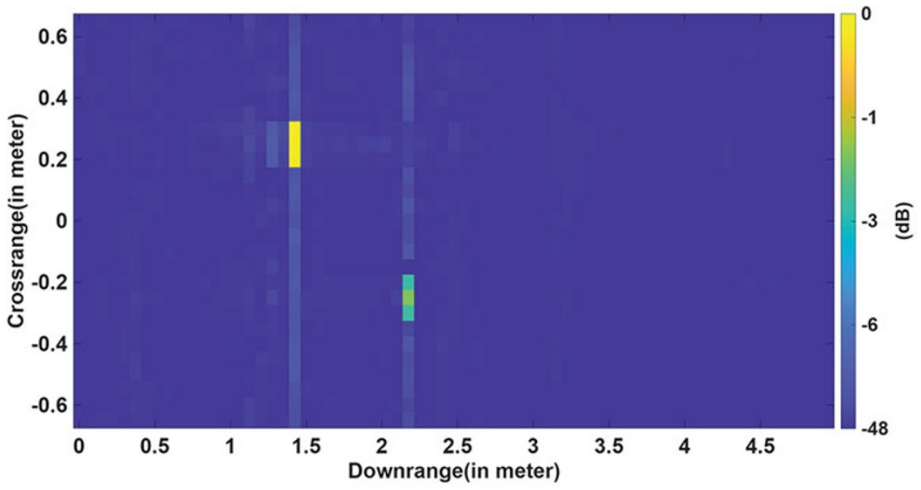
To evaluate the effectiveness of the proposed method, the proposed method was tested with real B-scan data obtained through an experiment. The experiment utilized SFCW radar, and the actual measurement system, as shown in Fig. 2, consisted of a horn antenna, a vector network analyzer, and a field scanner. A real building wall made up of bricks and covered by fine layer of plaster with a known thickness of 0.145 m and measured relative permittivity of 4.1 was examined. The radar was positioned 2.2 m away from the front side of the wall. Two TWRI scenarios were created and the target combinations are placed behind the wall: (i) In first scenario, a single metallic target with a very high dielectric constant was placed behind the wall. (ii) While in the second scenario, a combination of targets was used to create a contrast in dielectric properties. One target was wood, with a very low dielectric constant, while the other was metallic, with a much higher dielectric constant. Photographs of the targets and their measured radar cross-section (RCS) values are presented in Table 1. The RCS measurements for objects, such as metallic and wooden plates, were conducted using a step-frequency RCS measurement system. This system includes a network analyzer that transmits and receives step-frequency signals, a horn antenna for transmission and reception, high-performance absorbers in an anechoic chamber, and low scattering rigid supports made of low-density foam. The RCS measurement of targets using a quasi-monostatic configuration has been done as per the method described in Ref. [25].

Table 1. Detail of targets behind the wall

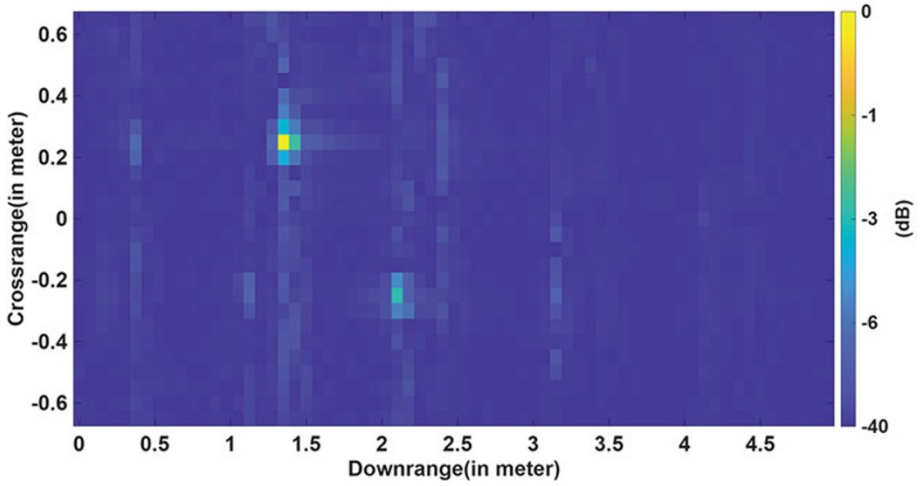
TWRI scenario	Actual image of target	RCS value (dBsm) [25]	Distance from wall (m)
1	 Target ID: T1 Metal(Size: 30 cm × 30 cm)	7.4	1.2
2	 Target ID: T2 Wood(Size: 30 cm × 30 cm)	−6.8	2.8
	 Target ID: T1 Metal (Size: 30 cm × 30 cm)	7.4	0.6

The data are collected using a stepped-frequency radar system operating within a frequency range of 3.5–5.5 GHz, with a frequency step size of 10 MHz [26]. This results in 201 frequency bins ($N = 201$). The scene is illuminated by an antenna as it moves horizontally across 27 scan positions ($M = 27$). The full data set, therefore, contains $M \times N$, or 27×201, which equals 5427 samples. The scattering parameter S_{11} was measured using the VNA

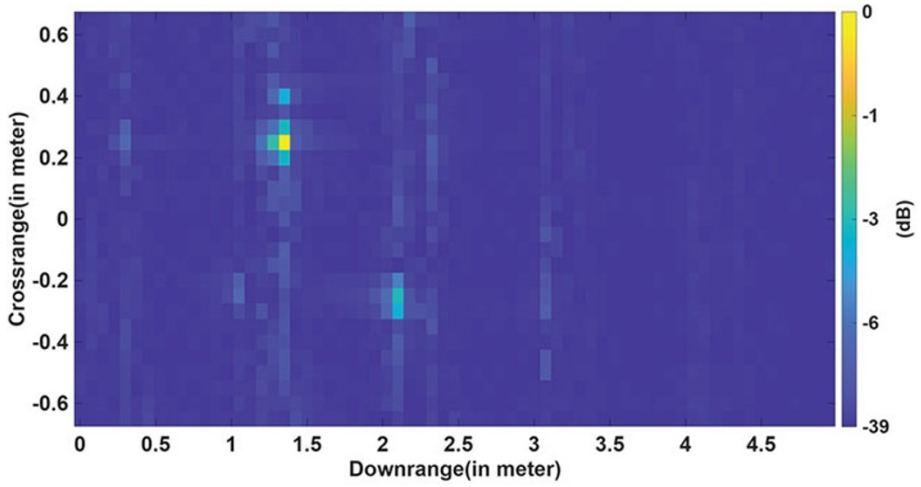
https://doi.org/10.1017/S1759078726103006 Published online by Cambridge University Press



(a) d=0.10 m



(b) d=0.18 m

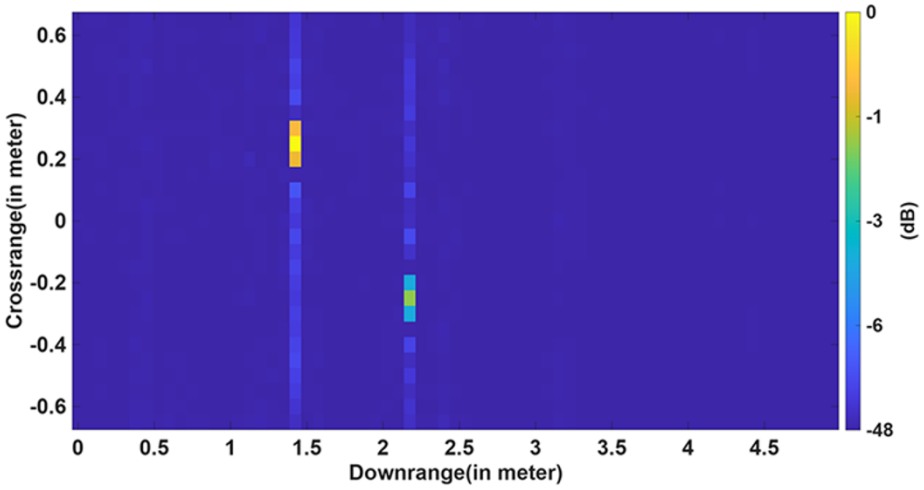


(c) d=0.27 m

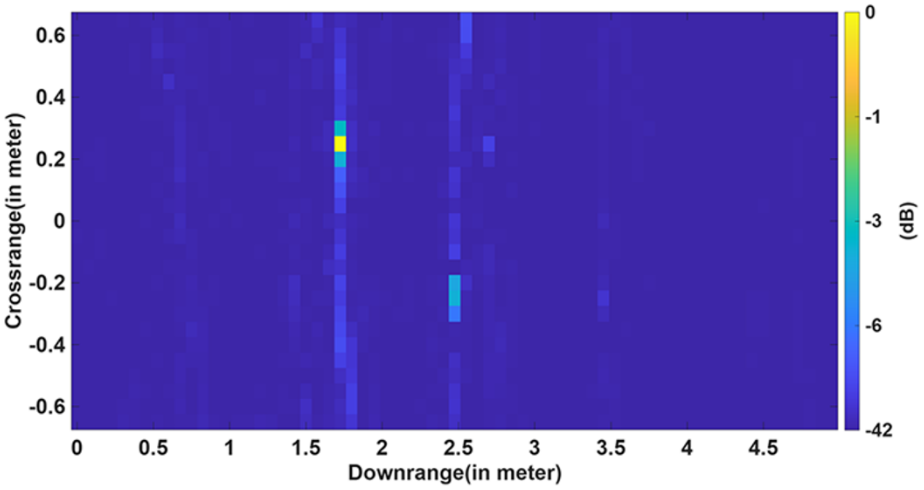
Figure 3. Reconstruction results at different thickness values (*d*) for Scene 1.

across 201 frequency points within the range of 3.5–5.5 GHz at 27 scan points along the horizontal direction. The wall is in the far-field region, allowing the assumption that the TEM wave is incident normally on the wall. The frequency domain data acquired is converted into the time domain to exploit the P_{t1} and estimate the relative permittivity value using Steps 1–4. The inverse Fourier transform converts frequency-domain data $E(m, f)$ into time-domain data, yielding the time response at each scan point. To remove antenna mismatch reflections, a reference signal $E_O(m, t)$ from an anechoic chamber is subtracted, leaving only reflections

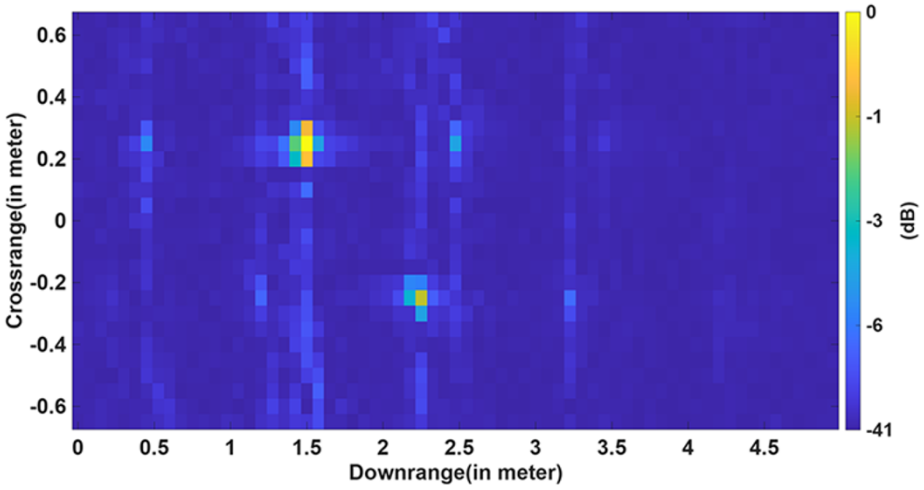
https://doi.org/10.1017/S1759078726103006 Published online by Cambridge University Press



(a) d=0.30 m



(b) d=0.11 m



(c) d=0.27 m

Figure 4. Reconstruction results at different thickness values (*d*) for Scene 2.

https://doi.org/10.1017/S1759078726103006 Published online by Cambridge University Press

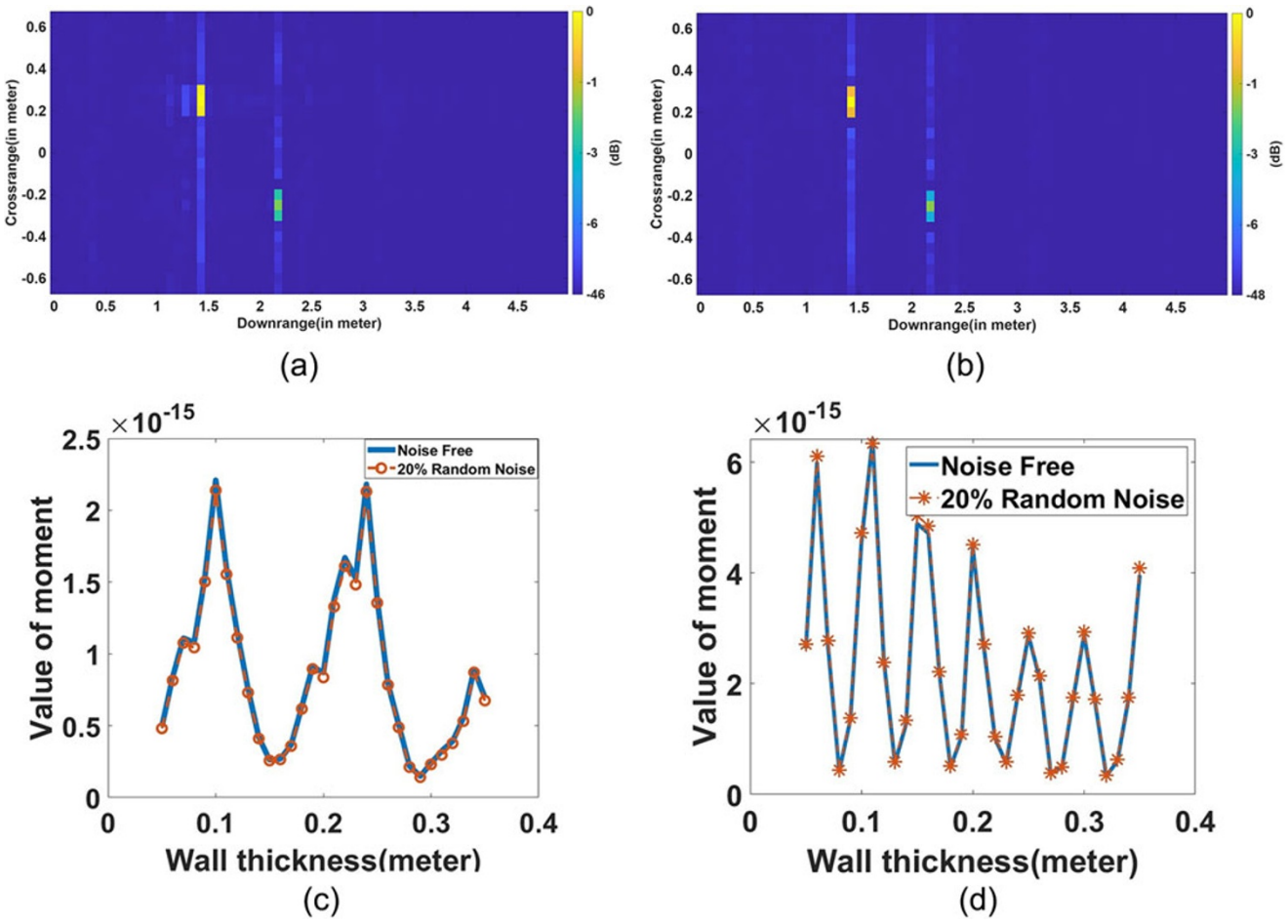


Figure 5. (a) Reconstruction results with 20% noise of Scene 1, (b) Reconstruction results with 20% noise of Scene 2, (c) Moment value plots with and without noise in the case of Scene 1, and (d) Moment value plots with and without noise in the case of Scene 2.

from the wall and targets. SVD was applied to separate the wall and target echoes. To obtain P_{t1} at time point t_1 for all scan points, $E_W(m,t)$ is summed in the time domain, the index t_1 corresponding to the maximum sum is identified, and P_{t1} at t_1 is determined from the time-domain profile for a selected scan point $m = 10$. From P_{t1}, the relative permittivity value of wall was estimated which was found to be 4.3. The results corresponding to Steps 1–4 are presented in Fig. 6(a–f).

Using the estimated relative permittivity, an image quality optimization scheme can be applied iteratively to achieve autofocus in the images. In each iteration, the assumed wall thickness value is modified, and a new beamformed image is generated based on the updated wall thickness. The thickness varies from 0.10 to 0.20 m. The optimal thickness value is determined at the moment when the moment value of the image reaches its maximum, and the corresponding image represents the final imaging result. Figure 7(a) and 7(c) displays the moment values at different thicknesses of Scenes 1 and 2. From the Fig. 7(a) and 7(c), it is clear that the value of the moment is maximum at the wall thickness of 0.15 m.

Figure 7(b) and 7(d) shows the reconstructed results with autofocusing of Scenes 1 and 2 when the thickness parameter is estimated as $d = 0.15$ m. Reconstructed results for Scene 1 and Scene 2, respectively, when the wall parameters are correctly known, are also shown in Fig. 7(e) and 7(f). It can be observed that the reconstructed images shown in Fig. 7(b) and 7(d) closely resembles with Fig. 7(e) and 7(f) demonstrate accurate target localization with well-focused images, confirming the effectiveness of the proposed algorithm. Thus, the proposed algorithm can yield high-quality focused imaging results. This simulation was conducted on a personal computer equipped with an Intel Core i7 processor and 16 GB of RAM in a MATLAB environment.

In addition, reconstruction results corresponding to incorrect relative permittivity and wall thickness values are also presented. Figure 8(a) shows the reconstruction obtained when the relative permittivity is incorrectly estimated as 6.5, with the maximum moment occurring at a thickness of 0.195 m. Consequently, the target is shifted from its true location in the radar image. Figure 8(b) and 8(c) presents the reconstructed images for Scene 2 at wall thickness values different from the true value, resulting in blurred and defocused images. It can be observed that using incorrect wall parameters during imaging can defocus the reconstructed image, leading to blurred or displaced target representations.

To further demonstrate the effectiveness of the proposed approach for 3D image reconstruction, experimental results are presented in this section. Using the same measurement setup, B-scan data were acquired at 21 different heights. The target T1 was

https://doi.org/10.1017/S1759078726103006 Published online by Cambridge University Press

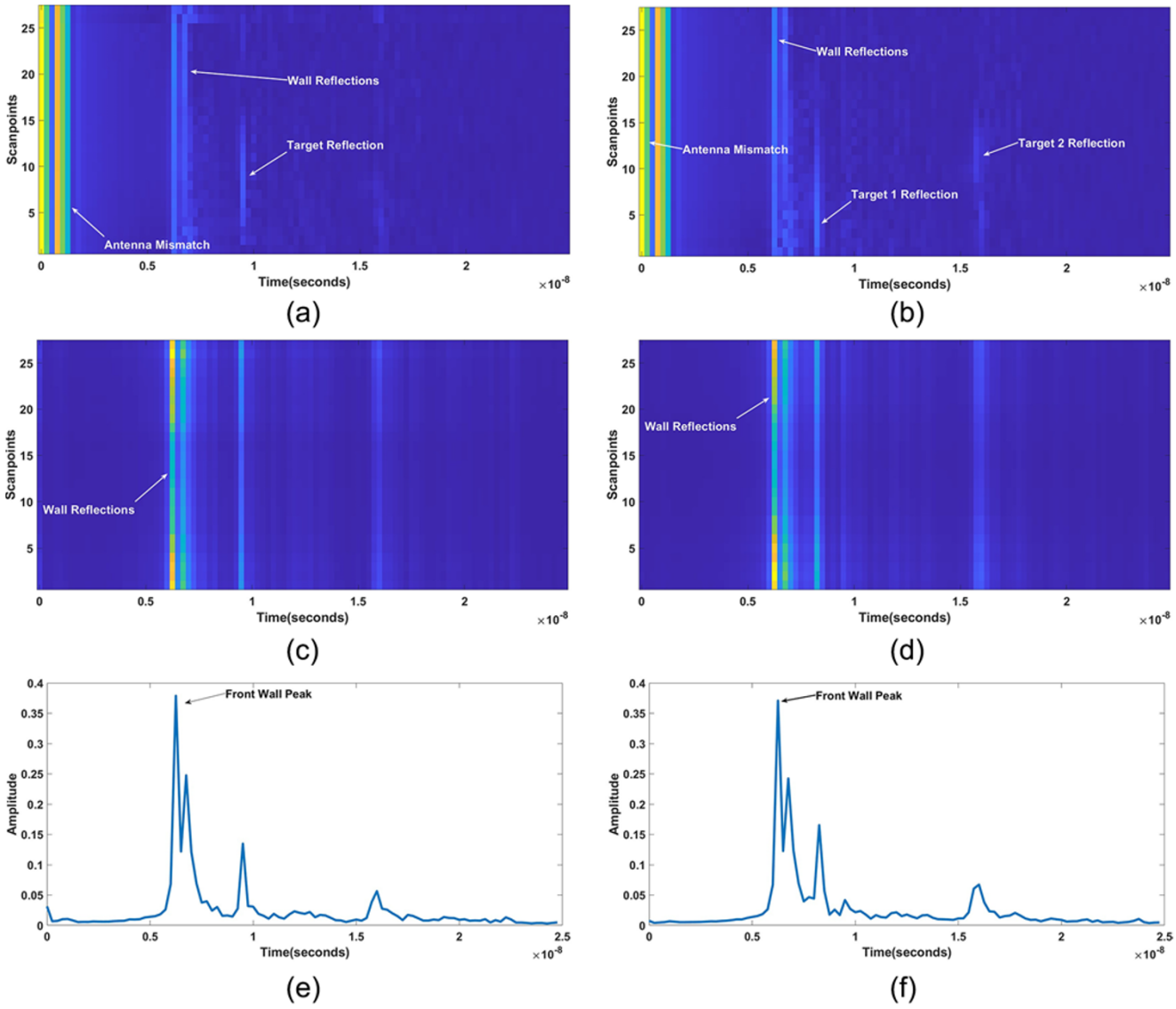


Figure 6. (a) Raw B-scan image of Scene 1 in time domain after Step 1, (b) Raw B-scan image of Scene 2 in time domain after Step 1, (c) B-scan image after application of background subtraction and SVD on Scene 1 using Steps 2 and 3, (d) B-scan image after application of background subtraction and SVD on Scene 2 using Steps 2 and 3, (e) Plot of sum after Step 4 of Scene 1, (f) Plot of sum after Step 4 of Scene 2.

positioned at a distance of 1.22 m behind the wall. In the first stage, the wall thickness and dielectric permittivity were estimated from the B-scan data at a selected height using the proposed autofocusing procedure. In the second stage, the estimated wall parameters were used to reconstruct 2D image slices at all heights. The measured data were first converted to the time domain, and background subtraction was performed following Steps 1 and 2. Step 3 was then applied to decompose the time-domain data into wall and target subspace components. In Step 4, Sum(t) was computed from the wall subspace, and the time instant t_1 corresponding to its maximum was identified. The results of Steps 1–4 are illustrated in Fig. 9(a–c).

Finally, in Step 5, the first wall reflection peak P_{t1} was obtained as $P_{t1} = S(m, t_1)$, and the wall's relative permittivity was estimated accordingly. Using the estimated permittivity, 2D slice radar images of size (27×67) pixels were reconstructed for wall thickness values ranging from 0.10 to 0.20 m, and the moment value was computed for each case. The optimal wall thickness was identified at the point where the moment value reached its maximum, and the corresponding image was selected as the final focused result. Figure 9(d) shows the autofocused 2D slice radar image corresponding to the maximum moment value. With the estimated wall parameters, all 2D slice reconstructions were combined to form a 3D representation of the concealed scatterers by superimposing the individual slices, yielding a volumetric image of the scene. The reconstructed 3D radar image result is shown in Fig. 10.

Comparison with other image quality-based autofocusing methods

The proposed method is compared with existing image quality-based autofocusing methods as shown in Table 2 in terms of computational cost, wall parameter search range, accuracy and reliability. The computational cost in Refs [2] and [8] is expressed

https://doi.org/10.1017/S1759078726103006 Published online by Cambridge University Press

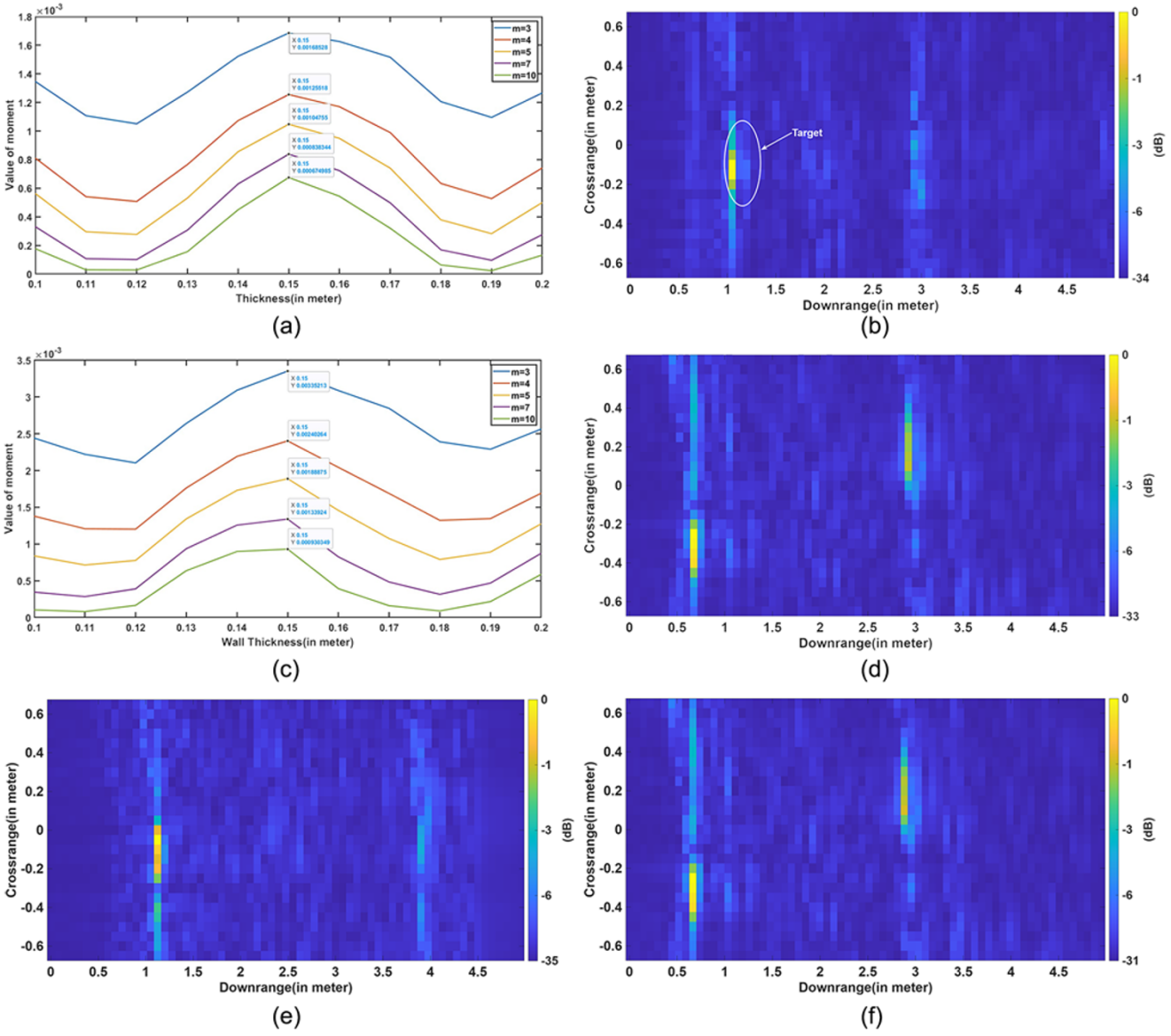


Figure 7. (a) Moment value at different thickness value for single target scene, (b) Reconstructed results with autofocusing for single target scene when the wall thickness is estimated as $d = 0.15$ m, (c) Moment value at different thickness value for contrast target scenario, (d) Reconstructed results with autofocusing for two target scenarios when the wall thickness is estimated as $d = 0.15$, (e) Reconstructed results with true wall parameter values for Scene 1, (f) Reconstructed results with true wall parameter for Scene 2.

as $O(N\varepsilon_r \cdot Nd \cdot Nx \cdot Ny \cdot Nz) + O(N\varepsilon_r \cdot Nd)$, because for each combination of relative permittivity (ε_r) and wall thickness (d), the algorithm reconstructs an image over all pixel points ($Nx \times Ny \times Nz$), and computes a focusing metric once per (ε_r, d) pair. The term $O(N\varepsilon_r \cdot Nd)$ appears because for each combination of relative permittivity (ε_r) and wall thickness (d), a total of $N\varepsilon \times Nd$ pairs, the algorithm evaluates a focus metric (e.g., entropy, sparsity, contrast), which typically returns a single scalar value used to identify the best (ε_r, d) combination. The computational cost of the proposed method is $O(Nd \cdot Nx \cdot Ny) + O(Nd)$ is calculated by reconstructing images over all pixel points ($Nx \times Ny$) for each wall thickness value (d), assuming ε_r is known, and performing a focus metric evaluation once per thickness value, contributing the additional $O(Nd)$ term. The computational cost is highest for $O(N\varepsilon_r \cdot Nd \cdot Nx \cdot Ny \cdot Nz) + O(N\varepsilon_r \cdot Nd)$, where both ε_r and d are unknown and image reconstruction and focus metric evaluation are performed for every (ε_r, d) pair and it is lowest for $O(Nd \cdot Nx \cdot Ny) + O(Nd)$ when ε_r is known, requiring reconstruction and evaluation only across different wall thickness values.

Limitations and future work

The proposed autofocusing method optimizes only wall thickness (d), reducing computational complexity for real-time radar applications. It enhances accuracy by estimating relative permittivity from time-domain reflections, minimizing errors from incorrect wall assumptions. The method improves feasibility with fewer iterations and single-variable optimization, making it ideal for security and search-and-rescue operations. It integrates seamlessly into TWRI systems without extra wall measurements. However, its effectiveness depends on an accurate initial ε_r estimate and

https://doi.org/10.1017/S1759078726103006 Published online by Cambridge University Press

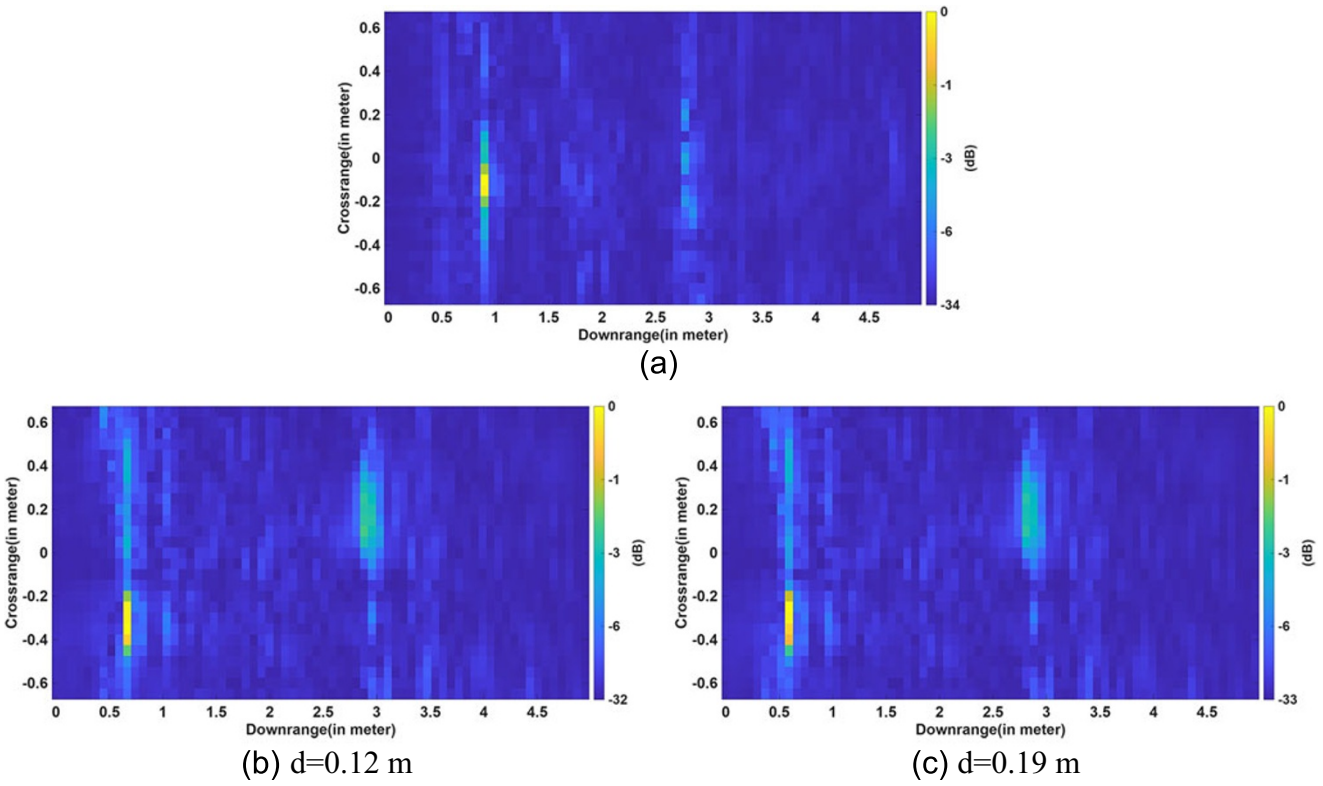


Figure 8. (a) Reconstructed results with autofocusing for single target scene when $\varepsilon_r = 2.7$ and $d = 0.11$ m, (b) Reconstructed result at thickness value = 0.12 m for Scene 2, (c) Reconstructed result at thickness value = 0.19 m for Scene 2.

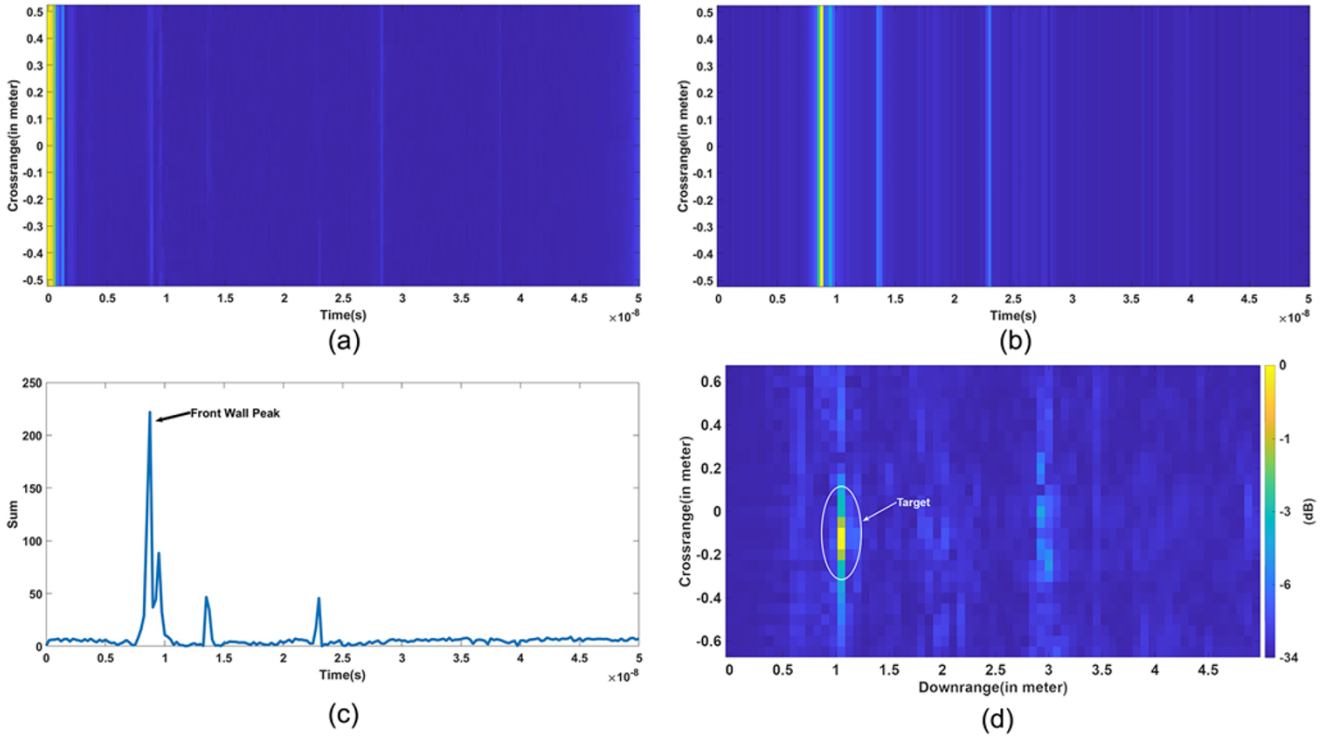


Figure 9. (a) Raw B-scan image after converting to time domain using Step 1, (b) B-scan image having wall reflections after applying Steps 2 and 3, (c) Sum of all A-scans along downrange Sum(t), (e) Autofocused 2D slice radar image corresponding to the maximum moment value.

https://doi.org/10.1017/S1759078726103006 Published online by Cambridge University Press

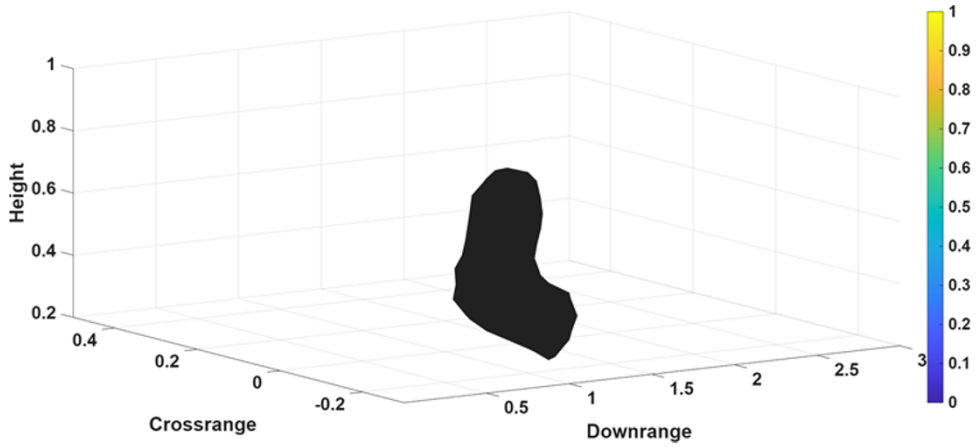


Figure 10. Reconstructed 3D radar image of the scene by superimposing the individual 2D radar image slices at different heights.

Table 2. Comparison of proposed method with other image quality-based autofocusing methods

Reference	Computational cost
[2]	$O(N\varepsilon_r \cdot Nd \cdot Nx \cdot Ny \cdot Nz) + O(N\varepsilon_r \cdot Nd)$
[8]	$O(N\varepsilon_r \cdot Nd \cdot Nx \cdot Ny \cdot Nz) + O(N\varepsilon_r \cdot Nd)$
Proposed method	$O(Nd \cdot Nx \cdot Nz) + O(Nd)$

$N\varepsilon_r$ = The number of values considered for relative permittivity (ε_r) of the wall, Nd = The number of values considered for wall thickness (d), Nx = The number of pixel points (or image points) in the x direction (horizontal), Ny = The number of pixel points (or image points) in the y direction (downrange), Nz = The number of pixel points (or image points) in the z direction (vertical).

remains untested in highly cluttered or dynamic environments. Moreover, the proposed method assumes that the wall can be modeled as a single homogeneous layer by clearly separating the front-wall and rear-wall echoes. This assumption is valid only when the wall is not electrically thin. In practice, the wall thickness must satisfy $d > \frac{c}{2(f_{max}-f_{min})\sqrt{\varepsilon_r}}$ to ensure reliable operation. Walls with thicknesses below this minimum limit violate the underlying assumption, which may degrade reconstruction accuracy. Additionally, it may not be suitable for multilayered walls, limiting its applicability in complex scenarios. Accurate wall parameter estimation is essential for optimizing transceiver placement and enhancing target resolution in TWRI systems [27, 28]. Future work will focus on developing a quantitative metric that integrates localization accuracy, spatial resolution, and contrast enhancement for a comprehensive assessment of imaging performance.

Conclusion

This paper presents an image autofocusing method for SAR-based 3D TWRI system. The approach begins by estimating the wall's relative permittivity from measurements. Using the estimated relative permittivity, it generates an autofocus image by adjusting only the wall thickness parameter. This method utilizes a single search variable, thereby minimizing the computational load on a real-time radar system. An experiment was conducted to evaluate the effectiveness of the proposed method. The experimental results confirm that the method successfully produces well-focused images, demonstrating its applicability in addressing the complexities related to real building walls.

Competing interests. The authors declare none.

References

1. **Nkwari PKM, Sinha S and Ferreira HC** (2018) Through-the-wall radar imaging: A review. *IETE Technical Review* **35**, 631–639. https://doi.org/10.1080/02564602.2017.1364146.
2. **Kaushal S, Kumar B and Singh D** (2019) An autofocusing method for imaging the targets for TWI radar systems with correction of thickness and dielectric constant of wall. *International Journal of Microwave and Wireless Technologies* **11**, 15–21. https://doi.org/10.1017/S1759078718001356.
3. **Wang F, Wu H, Qin T and Hong W** (2019) Parametric sparse representation for autofocused imaging through unknown walls. *International Journal of Remote Sensing* **40**, 5179–5191. https://doi.org/10.1080/01431161.2019.1579382.
4. **Ahmad F and Amin MG** (2006) Noncoherent approach to through-the-wall radar localization. *IEEE Transactions on Aerospace and Electronic Systems* **42**, 1405–1419.
5. **Wang G and Amin MG** (2006) Imaging through unknown walls using different standoff distances. *IEEE Transactions on Signal Processing* **54**, 4015–4025. https://doi.org/10.1109/TSP.2006.879325.
6. **Ertin E, Moses RL and Burkholder RJ** (2011) Autofocus for coherent through-the-wall imaging with multiple antenna arrays. In *2011 4th IEEE International Workshop on Computational Advances in Multi-Sensor Adaptive Processing (CAMSAP)*, 13-16 Dec. San Juan: IEEE, 69–72.
7. **Xin S, Biying L, Pengfei L and Zhimin Z** (2014) A multiarray refocusing approach for through-the-wall imaging. *IEEE Geoscience and Remote Sensing Letters*, **12**(4), 880–884.
8. **Xu Z, Jin T and Dai Y** (2022) Image domain filter for 3-D autofocusing of MIMO plane array in penetration scene. IEEE Geoscience and Remote Sensing Letters, **19**, 1–5.
9. **Solimene R, Soldovieri F, Prisco G and Pierri R** (2009) Three-dimensional through-wall imaging under ambiguous wall parameters. *IEEE Transactions on Geoscience and Remote Sensing* **47**, 1310–1317. https://doi.org/10.1109/TGRS.2009.2012698.
10. **Solimene R, Di Napoli R, Soldovieri F and Pierri R** (2011) TWI for an unknown symmetric lossless wall. *IEEE Transactions on Geoscience and Remote Sensing* **49**, 2876–2886. https://doi.org/10.1109/TGRS.2011.2110656.
11. **Zhang HM, Wang ZB, Wu ZH, Wang FF and Zhang YR** (2016) Real-time through-the-wall radar imaging under unknown wall characteristics using the least-squares support vector machines based method. *Journal of Applied Remote Sensing* **10**, 020501–020501. https://doi.org/10.1117/1.JRS.10.020501.
12. **Aftanas M, Sachs J, Drutarovsky M and Kocur D** (2009) Efficient and fast method of wall parameter estimation by using UWB radar system. *Frequenz* **63**, 231–235. https://doi.org/10.1515/FREQ.2009.63.11-12.231.

13. **Singh AP** (2024) A novel wall parameter estimation approach based on transmission line method from through-wall radar measurements. *Journal of Microwave Power & Electromagnetic Energy* **58**, 3–18. https://doi.org/10.1080/08327823.2024.2305485.
14. **Zhang HM, Zhang YR, Wang ZB, Wu ZH and Zhang CX** (2016) An efficient method based on machine learning for estimation of the wall parameters in through-the-wall imaging. *International Journal of Remote Sensing* **37**, 3061–3073. https://doi.org/10.1080/01431161.2016.1192703.
15. **Thajudeen C and Hoorfar A** (2016) A hybrid bistatic–monostatic radar technique for calibration-free estimation of lossy wall parameters. IEEE Antennas and Wireless Propagation Letters, **16**, 1249–1252.
16. **Qu L** (2020) Sparse blind deconvolution method for wall parameters estimation. IEEE Geoscience and Remote Sensing Letters, **19**, 1–5.
17. **Li L, Zhang W and Li F** (2010) A novel autofocusing approach for real-time through-wall imaging under unknown wall characteristics. *IEEE Transactions on Geoscience and Remote Sensing* **48**, 423–431. https://doi.org/10.1109/TGRS.2009.2024686.
18. **Ahmad F, Amin MG and Mandapati G** (2007) Autofocusing of Through-the-Wall Radar Imagery Under Unknown Wall Characteristics. *IEEE Transactions on Image Processing* **16**, 1785–1795. https://doi.org/10.1109/TIP.2007.899030.
19. **Gu X and Zhang Y** (2010) Autofocus imaging simulation for through-wall radar by using FDTD with unknown wall characteristics. In *2010 Asia-Pacific Microwave Conference*. 7-10 Dec, Yokohama, Japan. IEEE, 1657–1660.
20. **Jin T, Chen B and Zhou Z** (2012) Image-domain estimation of wall parameters for autofocusing of through-the-wall SAR imagery. *IEEE Transactions on Geoscience and Remote Sensing* **51**, 1836–1843. https://doi.org/10.1109/TGRS.2012.2206395.
21. **Zhuo X and Jin T** (2021) An image-domain filter for refraction effects compensation of penetrating MIMO imagery. *IEEE Geoscience and Remote Sensing Letters*, **19**, 1–5.
22. **Akhter Z and Akhtar MJ** (2016) Free-space time domain position insensitive technique for simultaneous measurement of complex permittivity and thickness of lossy dielectric samples. *IEEE Transactions on Instrumentation and Measurement* **65**, 2394–2405. https://doi.org/10.1109/TIM.2016.2581398.
23. **Protiva P, Mrkvica J and Machác J** (2011) Estimation of wall parameters from time-delay-only through-wall radar measurements. *IEEE Transactions on Antennas and Propagation* **59**, 4268–4278. https://doi.org/10.1109/TAP.2011.2164206.
24. **Tivive FHC, Bouzerdoum A and Amin MG** (2014) A subspace projection approach for wall clutter mitigation in through-the-wall radar imaging. *IEEE Transactions on Geoscience and Remote Sensing* **53**, 2108–2122. https://doi.org/10.1109/TGRS.2014.2355211.
25. **Hu CF, Xu JD, Li NJ and Zhang LX** (2008) Indoor accurate RCS measurement technique on UHF band. *Progress in Electromagnetics Research* **81**, 279–289. https://doi.org/10.1159/000151404
26. **Gaikwad AN, Singh D and Nigam MJ** (2011) Application of clutter reduction techniques for detection of metallic and low dielectric target behind the brick wall by stepped frequency continuous wave radar in ultra-wideband range. *IET Radar, Sonar & Navigation* **5**, 416–425. https://doi.org/10.1049/iet-rsn.2010.0059.
27. **Maisto MA, Masoodi M, Pierri R and Solimene R** (2022) Sensor arrangement in through-the-wall radar imaging. *IEEE Open Journal of Antennas and Propagation* **3**, 333–341. https://doi.org/10.1109/OJAP.2022.3159279.
28. **Maisto MA, Masoodi M and Solimene R** (2022) Transverse resolution in through-the-wall radar imaging. *URSI Radio Science Letters* **4**. https://doi.org/10.46620/22-0014.



Dr Akhilendra Pratap Singh received the PhD degree in Electronics Engineering from the Indian Institute of Technology (BHU), Varanasi, India. He is presently serving as an assistant professor in the Department of Electronics and Communication Engineering at Indian Institute of Information Technology Bhopal. His research interests include radar signal and image processing. He has published various research articles in reputed international journals and conferences.



Dr Vineet Singh received the PhD degree in Electronics Engineering from the Indian Institute of Technology (BHU), Varanasi, India. He is currently an assistant professor in the Department of Electronics and Communication Engineering at the National Institute of Technology (NIT), Patna. Prior to this, he was a Postdoctoral Research Associate at the Indian Institute of Technology (IIT), Roorkee. His research interests include Doppler signal processing, microwave-based ranging and target localization, microwave imaging for biomedical diagnostics, and nondestructive testing using microwave and millimeter-wave (mmWave) technologies. He has published research articles in reputed international journals and conferences and has also contributed book chapters and patents. He is a member of IEEE and other professional societies.

https://doi.org/10.1017/S1759078726103006 Published online by Cambridge University Press